PAPER

Surface engineered CoP/Co₃O₄ heterojunction for high-performance bi-functional water splitting electro-catalysis†

Xintong Li, [ID] [a] Yizhe Liu,[a] Qidi Sun,[a] Wei-Hsiang Huang,[b,c] Zilong Wang, [ID] [d] Chu-Chen Chueh, [ID] [e] Chi-Liang Chen [ID] [c] and Zonglong Zhu [ID] *[a]

In the electrochemical water splitting process, integrating hydrogen evolution reaction (HER) and oxygen evolution reaction (OER) in the same electrolyte with the same catalyst is highly beneficial for increasing the energy efficiency and reducing the fabrication cost. However, most OER catalysts are unstable in the acidic solution, while HER shows poor kinetics in the alkaline solution, which hinders the scale-up application of electro-catalytic water splitting. In this work, a CoP/Co₃O₄ heterostructure is firstly fabricated and then O and P defects are introduced *via* surface engineering (s-CoP/Co₃O₄). The as-prepared material was employed as the catalyst towards electrochemical water splitting in an alkaline environment. In alkaline HER, a current density of −10 mA cm⁻² can be achieved at an overpotential of 106 mV *vs.* RHE. In the OER process, the overpotential of s-CoP/Co₃O₄ electrode is only 211 mV *vs.* RHE at 10 mA cm⁻² in 1 M KOH, and the corresponding Tafel slope is only 58.4 mV dec⁻¹ so that the s-CoP/Co₃O₄ electrode could be used as the bifunctional catalyst for alkaline water splitting. This work provides a simple and low-cost approach to fabricate a Co-based heterojunction electrode with unsaturated metal sites to improve the electro-catalytic activities towards water splitting.

Introduction

Renewable energy has been growing rapidly as over 80% of the global energy consumption relies on nonrenewable fossil fuels.[1] As promising energy revolutions, wind and solar can generate electricity with zero pollutant emissions.[2] However, how to utilize the engendered clean energy is limited by the sustainable energy storage and their scaled application.[3] Compared with various energy storage technologies, electro-catalytic water splitting provides a possible strategy as an intermediate approach for energy storage and conversion.[4] To efficiently operate the water splitting process, a large activation energy barrier for both hydrogen evolution reaction (HER) and oxygen evolution reaction (OER) needs to be overcome.[5,6] Noble metals based catalysts will benefit the water splitting kinetics for efficient HER and OER,[7] but their widespread application has been limited by their high cost and scarcity in practical processes.[8] Thus, it is necessary to develop high-performance catalysts for water splitting with earth-abundant materials.

For practical applications, bifunctional HER and OER electro-catalysis can significantly increase energy utilization and reduce electrode costs.[9] Although impressive progress has been made, only a few high-performance electrocatalysts with bifunctional HER and OER catalytic activity in the same electrolyte have been reported. As most of the catalysts have poor stability in acid solution, it is highly attractive to develop high-performance non-noble bifunctional electro-catalysts for overall water splitting in alkaline environment.[10,11]

Cobalt-based materials have been widely reported as the electro-catalysts for water splitting.[12] Typically, cobalt oxides (CoOₓ) have performed efficiently during the OER process, thanks to accessible adsorption sites from electro-deficient Co 3d orbits.[11] Their oxygen vacancies facilitate the pre-oxidation of the adjacent Co atoms and the formation of Co–OOH during the OER process, further boosting the catalytic activi-

[a]Department of Chemistry, City University of Hong Kong, Kowloon, 999077, Hong Kong. E-mail: zonglzhu@cityu.edu.hk
[b]Graduate Institute of Applied Science and Technology, National Taiwan University of Science and Technology (NTUST), Taipei 10607, Taiwan
[c]National Synchrotron Radiation Research Centre, Hsinchu 30076, Taiwan, Republic of China
[d]Siyuan Laboratory, Guangdong Provincial Engineering Technology Research Centre of Vacuum Coating Technologies and New Energy Materials, Department of Physics, Jinan University, GuangzhouGuangdong 510632, P. R. China
[e]Department of Chemical Engineering, National Taiwan University, Taipei 10617, Taiwan
†Electronic supplementary information (ESI) available. See DOI: 10.1039/d1nr06044a

ties of cobalt oxides towards oxygen evolution.[13] Their oxygen vacancies facilitate the pre-oxidation of the adjacent Co atoms and the formation of Co–OOH during the OER process, further boosting the catalytic activities of cobalt oxides towards oxygen evolution.[14] However, simple CoO_x exhibited deficient catalytic activity under HER operation. On the contrary, CoP containing electronegative P atoms, which offer adsorption sites towards electropositive reactants and intermediate,[6,15,16] is considered as a suitable catalytic candidate for HER.[14] However, the H_2 desorption process has been impeded due to the strong binding between CoP and H atoms, which further results in poor performance.

In this work, we firstly designed and synthesized COP/ Co_3O_4 heterostructure by an electro-deposition method. To improve the electro-catalytic properties both under the HER and OER processes, we introduced oxygen and phosphorus vacancies into the COP/Co_3O_4 heterostructure using a partial reduction process, respectively. The surface engineered COP/ Co_3O_4 (s-COP/Co_3O_4) was then characterized using Raman, X-ray diffraction (XRD), transmission electron microscopy (TEM), and X-ray photoelectron spectroscopy (XPS). The results show that the CoP nanosheets grow vertically and uniformly on the surface of the Co_3O_4 layers, and the ratio of Co_2^+/Co^{3+} increased after the reduction process. s-COP/Co_3O_4 shows a much better catalytic performance than pristine COP/Co_3O_4, a current density of 10 mA cm^{-2} can be achieved at an overpotential of 211 mV *vs.* RHE in the OER process and the overpotential is only 106 mV *vs.* RHE at a current density of −10 mA cm^{-2} in HER, which surpasses most of the transition metal-based catalysts from the previously reported works. X-ray absorption spectroscopy (XAS) was also employed to further explain the elevated performances after the surface engineering process, the results show the successful formation of P vacancies in CoP. Different effects of the heterojunction struc-

ture in HER and OER are also presumed in the s-COP/Co_3O_4 system. This work provides a feasible approach to fabricate a low-cost, high-performance bi-functional electrocatalyst for HER and OER as well as verifying the positive effects of the heterojunction structure and surface engineering process.

Results and discussion

The fabrication process of the s-CoP/Co_3O_4 electrode is illustrated in Fig. 1a. $Co(OH)_2$ was first obtained by precipitation and then thermally treated in the air at 250 °C to obtain Co_3O_4. The black Co_3O_4 powder was coated on the carbon paper and then electro-deposited in the electrolyte containing Co_2^+, $H_2PO_4^{2-}$ and sequestrant (sodium citrate) at −1.0 V for 900 s to involve CoP. The CoP-coated Co_3O_4 electrode was soaked in a freshly-prepared $NaBH_4$ solution (0.5 M) to obtain the final s-CoP/Co_3O_4 electrode.

Raman spectra of Co_3O_4 and s-Co_3O_4 were recorded to analyze the variation of crystal structure and increase of surface defects. As shown in Fig. 1b, the bands at 186, 470, 510 and 676 cm^{-1} correspond to the $F_{2g}^{(1)}$, E_{2g}, $F_{2g}^{(2)}$ and A_{1g} symmetries, respectively, of Co_3O_4.[17] The peak of A_{1g} symmetry in the Raman spectrum of Co_3O_4 negatively shifts from 676 to 668 cm^{-1}, which indicates that more defects are created during surface engineering of Co_3O_4, thus verifying the successful involvement of oxygen vacancies after $NaBH_4$ reduction.[18] The XRD patterns of Co_3O_4, s-Co_3O_4, CoP/carbon paper and bare carbon paper are shown in Fig. 1c. The diffraction peaks at 19.0°, 31.3°, 36.8°, 59.4° and 65.3° can be ascribed to (111), (220), (311), (400) and (440) planes of the cubic Co_3O_4, respectively. After the reduction treatment, the crystal structure remained in the s-Co_3O_4 structure, indicating that there was no crystal phase variation compared with Co_3O_4. The intense peaks at 23.8° and 26.4° of CoP/carbon
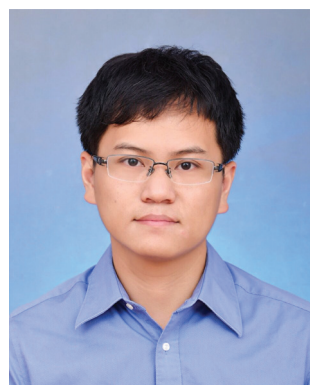
Since joining in CityU, Dr Zonglong Zhu has established optoelectronic materials and devices lab. Until now, more than 30 articles have been published as corresponding author, including Nat. Nano*,* Nat. Commun.*,* J. Am. Chem. Soc.*,* Adv. Mater.*,* Adv. Energy Mater.*,* Adv. Funct. Mater.*,* Adv. Sci.*,* Joule*, and* Small Methods*, and one US patent has been filed. His research mainly focuses on the design in-*

Zonglong Zhu

organic/organic materials, as well connecting the materials synthesis, physical properties and device performance for optoelectronics application. The current application interests include solar cells, transistors, light-emitting diodes, and electrochemical devices (e.g. batteries, supercapacitors).
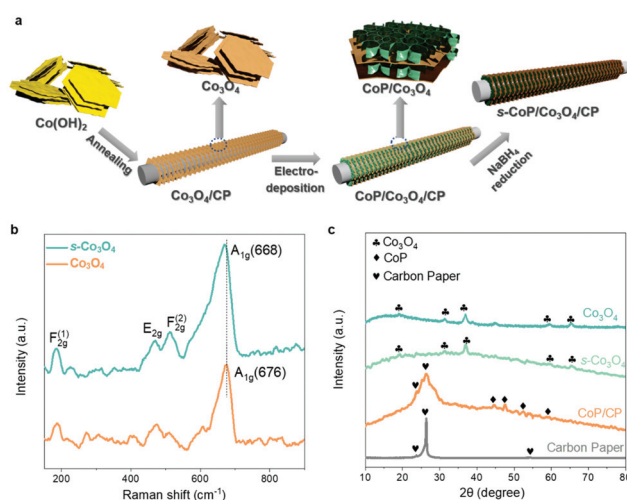

Fig. 1 (a) Illustration of the preparation process of s-CoP/Co_3O_4. (b) Raman spectra at the wave length of 532 nm of Co_3O_4 and s-Co_3O_4. (c) XRD patterns of Co_3O_4, s-Co_3O_4, CoP/carbon paper, and carbon paper.

paper electrode correspond to the peaks of the carbon paper at 46.2°, 48.1°, 52.3° and 56.7° correspond to (112), (211), (103) and (301) peaks of CoP. SEM images of Co_3O_4, s-Co_3O_4, CoP electrodeposited at different potentials (−0.8, −1.0 and −1.5 V vs. RHE) and s-CoP/Co_3O_4 are shown in Fig. S1.† The results show that Co_3O_4 is of the layered structure. After the $NaBH_4$ reduction process, pores appeared on the surface of s-Co_3O_4. The electro-deposited CoP also had a nanolayered structure and the thickness of the CoP layer was the smallest when the deposition potential was −1.0 V vs. Ag/AgCl. The SEM image of s-CoP/Co_3O_4 showed that the CoP layers grew vertically on the surface of the Co_3O_4 layer, forming a three-dimensional connected structure, facilitating the transfer processes, and creating more exposed active sites.

The high-resolution transmission electron microscopy (HR-TEM) image of the s-CoP/Co_3O_4 electrode is shown in Fig. 2a and the interplanar distances of CoP and Co_3O_4 are demonstrated in Fig. 2b$_{1-3}$. The lattice fringes of 0.283, 0.244 and 0.202 nm indicate the (011) facet of CoP and (113), (400) facets of Co_3O_4, respectively.[19] The elemental mapping result of s-CoP/Co_3O_4 (Fig. 2c–f) shows that Co, O and P atoms are distributed uniformly on the surface of the electrode, suggesting that the CoP nanolayers grow homogeneously on the surface of Co_3O_4.

The elemental compositions and chemical states of the as-prepared Co_3O_4, s-Co_3O_4, CoP, CoP/Co_3O_4 and s-CoP/Co_3O_4 were further analyzed from XPS spectra (Fig. 3). High-resolution XPS spectra of Co 2p in Co_3O_4 and s-Co_3O_4 are shown in Fig. 3a. The major peaks at about 795 and 780 eV can be ascribed to Co $2p_{1/2}$ and Co $2p_{3/2}$, respectively, both of which could be deconvoluted to the peaks of Co^{2+} (782.2 and 796.9 eV) and Co^{3+} (779.88 and 794.9 eV), and the additional peaks at 788.5 and 804.2 eV are satellite peaks.[20] The Co^{2+}/Co^{3+} ratios are estimated to be 50.2% and 54.6% in Co_3O_4 and s-Co_3O_4, respectively, according to the relative area of the deconvoluted peaks corresponding to Co^{2+} and Co^{3+}. The detailed calculation process is shown in the ESI.† It has been reported that
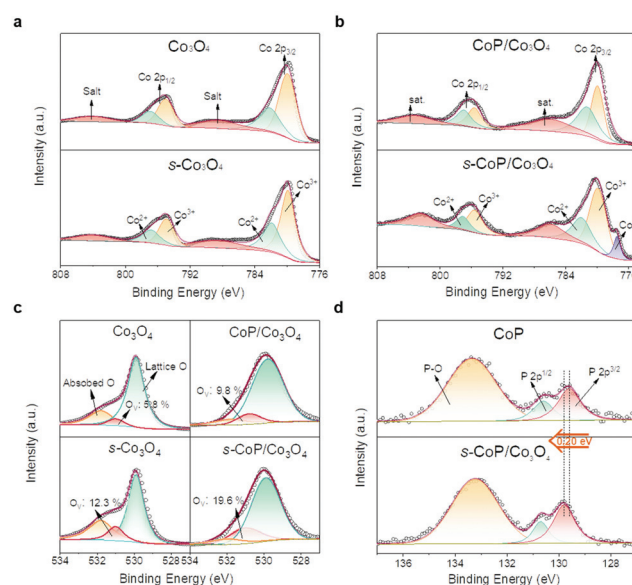

Fig. 3 High-resolution XPS spectra of Co 2p in (a) Co_3O_4, s-Co_3O_4, (b) CoP/Co_3O_4 and s-CoP/Co_3O_4. High-resolution XPS spectra of (c) O 1s in Co_3O_4, s-Co_3O_4, CoP/Co_3O_4 and s-CoP/Co_3O_4, and (d) P 2p in CoP and CoP/Co_3O_4.

$NaBH_4$ will react with Co_3O_4 during the surface engineering process,[15] making Co_3O_4 remaining at the oxygen-deficient states, thus the ratio of Co^{2+} will increase to achieve charge balance in s-Co_3O_4.[22] Therefore, the increased ratio of Co^{2+}/Co^{3+} indicates the successful reduction of Co_3O_4 by the $NaBH_4$ treatment. The high-resolution XPS spectra of Co 2p of CoP/Co_3O_4 and s-CoP/Co_3O_4 from Fig. 3b show that the peak of Co^0 appears at 777.5 eV after reduction, suggesting a small amount of CoP was reduced to Co by $NaBH_4$.[11] Schottky junction structures are formed at the interface of Co and CoP, facilitating electrons transfer from Co to CoP according to the Mott–Schottky effect, thus further facilitating the OER process.[21]
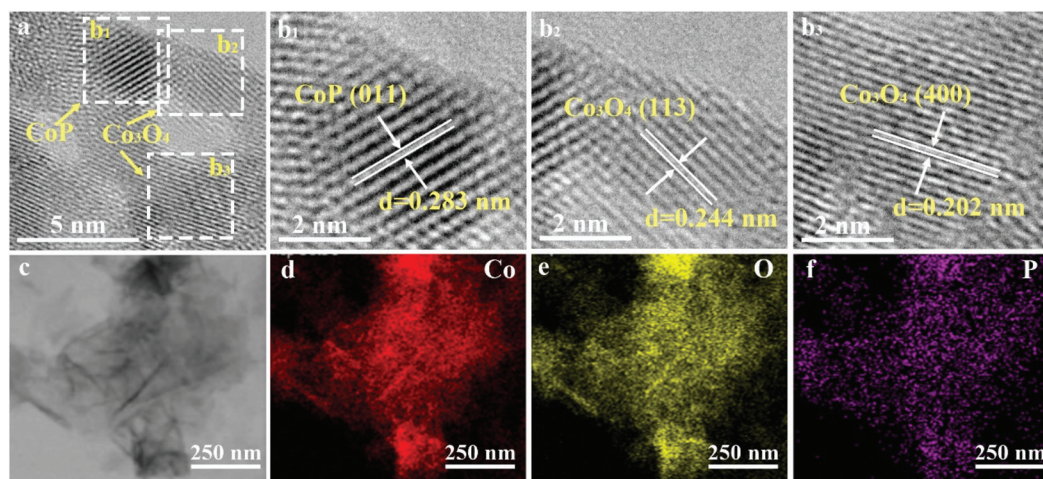

Fig. 2 (a) HR-TEM image of s-CoP/Co_3O_4, corresponding lattice fringe images of (b$_1$) CoP and (b$_2$–b$_3$) Co_3O_4, (c–f) TEM elemental mapping of s-CoP/Co_3O_4 electrode.

The O 1s high-resolution XPS spectra of the as-prepared materials could be deconvoluted to three peaks in Co_3O_4, s-Co_3O_4, CoP/Co_3O_4 and s-CoP/Co_3O_4 (Fig. 3c). The peaks at 529.9, 531.0 and 531.8 eV correspond to the O atoms coordinating with metal species (lattice O), surface oxygen defect species (O_V) and O from adsorbed molecular water (absorbed O), respectively.[22] The peaks corresponding to the adsorbed O exist in Co_3O_4 and s-Co_3O_4 because they absorbed water molecules from the air. However, the peak areas corresponding to the absorbed O in CoP/Co_3O_4 and s-CoP/Co_3O_4 decrease because they are characterized when coated on the carbon paper while the XPS signals of Co_3O_4 and s-Co_3O_4 were obtained from the powder sample. Moreover, the ratio of O_V increases from 5.8% in Co_3O_4 to 12.3% in s-Co_3O_4, verifying the involvement of oxygen vacancies. With the protection of the electro-deposited CoP, the ratio of O_V also increases from 9.8% to 19.6% after the reduction process. In Fig. 3d, the high-resolution XPS spectra of P 2p can be deconvoluted to three peaks. The binding energies of 129.6 and 130.6 eV can be attributed to $2p_{3/2}$ and $2p_{1/2}$ while the peak at 133.3 eV is ascribed to the surface oxidized P species, indicating the successful involvement of CoP.[23] Moreover, the peak corresponding to P $2p_{3/2}$ was positively shifted by 0.20 eV after the reduction process, signifying fewer electrons occupied P atoms, which facilitates the H* desorption in the HER process.[24] The ΔG_{H^*} value of CoP is much negative, in other words, H* adsorbs too strongly on the surface of CoP, so that the H* desorption is the rate-determining step of the HER process. Therefore, the catalytic activity of CoP towards HER will be enhanced after the partial reduction procedure.

The electro-catalytic activities of the as-prepared materials towards water splitting (OER and HER) are tested in the alkaline electrolyte (1 M KOH) with a conventional three-electrode system. The polarization curves were recorded using linear sweep voltammetry (LSV) at a scan rate of 5 mV s⁻¹. As shown in Fig. 4a, the Co_3O_4/carbon paper (Co_3O_4/CP) electrode carries a limited catalytic efficiency towards OER, while s-Co_3O_4/CP performs better activity owing to the larger number of oxygen vacancies. The dosage of $NaBH_4$ was adjusted to optimize the reduction conditions of Co_3O_4 and the result is shown in Fig. S2.† The catalytic performance of s-Co_3O_4 improves when the concentration of $NaBH_4$ increases from 0.3 M to 0.5 M yet it gets poorer when the concentration of $NaBH_4$ further increases to 0.7 M, owing to the impaired conductivity of Co_3O_4 caused by excessive oxygen vacancies. This conclusion can be further verified by the increased Tafel slope (from 63.8 mV dec⁻¹ of 0.5-Co_3O_4 to 82.1 mV dec⁻¹ of 0.7-Co_3O_4, Fig. S3†). The involvement of CoP enhances the catalytic performance of Co_3O_4 to a large extent, the overpotential of CoP/Co_3O_4 was decreased to 298 mV at a current density of 10 mA cm⁻². The deposition time of CoP was also adjusted to optimize the catalytic efficiency of CoP/Co_3O_4, which is shown in Fig. S4,† and the electro-catalytic performance of CoP/Co_3O_4 was the best when the deposition time was 900 s. The electro-catalytic efficiency could be further enhanced while the CoP was coated on the surface engineered Co_3O_4, obtaining an overpotential of 265 mV at 10 mA cm⁻². s-CoP/

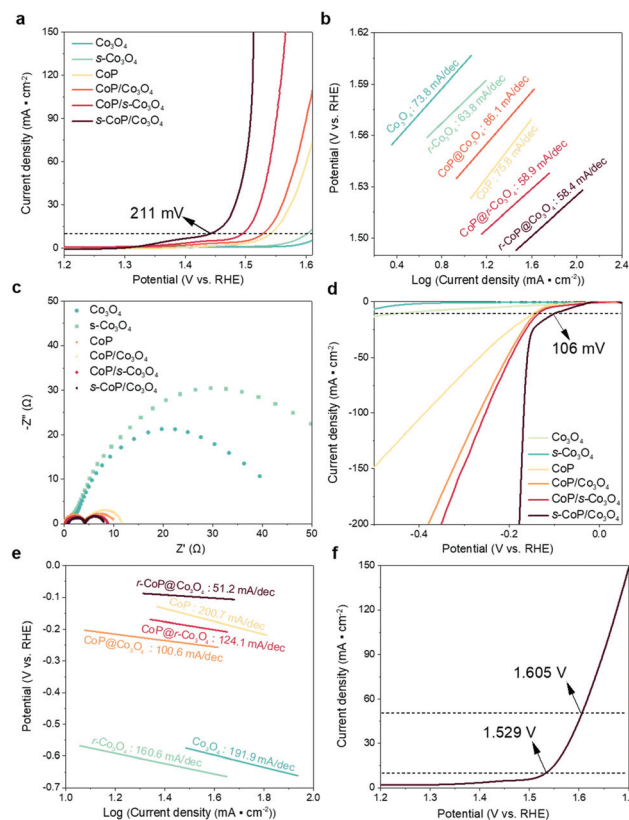
Fig. 4 (a) OER polarization curves, (b) corresponding Tafel plots (c) EIS (@−0.2 V vs. RHE) spectra, (d) HER polarization curves and (e) corresponding Tafel plots of Co_3O_4, s-Co_3O_4, CoP, CoP/Co_3O_4, CoP/s-Co_3O_4 and s-CoP/Co_3O_4 in 1 M KOH, (f) water splitting polarization curves of s-CoP/Co_3O_4 in 1 M KOH.

Co_3O_4 realizes the earliest overpotential of 211 mV at 10 mA cm⁻² and the smallest Tafel slope (58.4 mV dec⁻¹) (Fig. 4b), surpassing the performance of IrO_2/carbon paper (281 mV, Fig. S5†). The electrochemical impedance spectroscopy (EIS) spectra of the electrodes were recorded at −0.2 V vs. RHE and 1.6 V vs. RHE and the results are shown in Fig. 4c and Fig. S10.† The impedance of Co_3O_4 is slightly enlarged after the reduction process, indicating an impaired electron transfer property though more exposed active sites are created after the reduction process. The impedances of CoP, CoP/Co_3O_4 and s-CoP/Co_3O_4 are much smaller than that of Co_3O_4 and s-Co_3O_4, further verifying that the involvement of CoP layers improves the electrons transfer properties to a large extent.

The HER performance of samples were also investigated under alkaline conditions (1 M KOH). As shown in Fig. 4d, Co_3O_4 and s-Co_3O_4 electrodes showed poor catalytic activities towards HER as expected. With the involvement of the CoP layer, the overpotentials of CoP/Co_3O_4 and s-CoP/Co_3O_4 towards HER get much earlier, because the involved CoP offers the effective adsorption sites towards electropositive reactants and intermediates. Moreover, these two materials also perform better than the CoP, which is attributed to the water dissociation effects of Co_3O_4. Similar to OER systems, the earliest

overpotential at 10 mA cm^{-2} was obtained for s-CoP/Co$_3$O$_4$ (106 mV), and the corresponding Tafel slope was only 51.2 mV dec^{-1} (Fig. 4e), which is close to the performance of Pt/C/ carbon paper (56 mV, Fig. S6†). The much-elevated performance can mainly be attributed to two aspects, (1) P defects further optimize the electronegativity of CoP and (2) s-Co$_3$O$_4$ catalyzes the water dissociation efficiently. Due to the outstanding electrocatalytic activity of the s-CoP/Co$_3$O$_4$ electrode towards both HER and OER, it was adopted as the bifunctional catalyst in the water splitting cell. The water spitting performance of s-CoP/Co$_3$O$_4$ was recorded in a two-electrode system. As presented, to offer the current densities of 10 and 50 mA cm^{-2}, the cell potentials were only 1.529 and 1.605 V, respectively (Fig. 4f), which surpass those reported for most of the electrodes in the latest journals (Table S3† and Fig. 5e).

The durability of the s-CoP/Co$_3$O$_4$ electrode is verified by the LSV polarization before/after 5000 CV cycles at a scan rate of 50 mV s^{-1} and current–time (i–t) curves conducted at 211 mV (overpotential of OER at 10 mA cm^{-2}) and −106 mV (overpotential of HER at −10 mA cm^{-2}), respectively. As shown in Fig. 5a and b, no obvious deactivation could be observed after 5000 CV cycles in both OER and HER systems. Moreover, the current density barely shows any attenuation after operat-

ing at fixed overpotentials for 24 h. The electrochemical double-layer capacitances (C_{dl}s, Fig. 5c) of the Co$_3$O$_4$, CoP, CoP/Co$_3$O$_4$ and s-CoP/Co$_3$O$_4$ electrodes were calculated according to the cyclic voltammograms (CVs, Fig. S7†) at different scan rates (10 to 100 mV s^{-1}). The results show that the C_{dl} of s-CoP/Co$_3$O$_4$ (28.5 mF cm^{-2}) is much larger than that of Co$_3$O$_4$ (1.02 mF cm^{-2}), CoP (1.13 mF cm^{-2}) and CoP/Co$_3$O$_4$ (1.99 mF cm^{-2}). As well established, C_{dl} of the material is proportional to its electrochemically active surface areas (ECSA).[25] Therefore, the C_{dl} results indicate that the coated CoP layer increases the ECSA of Co$_3$O$_4$ and the reduction process further enlarges the ECSA of CoP/Co$_3$O$_4$ to a larger extent, which can be attributed to the involvement of unsaturated cationic sites, they act as active sites and facilitate the pre-oxidation of the low valence Co and initiate OER at a lower applied potential. Therefore, the reduction process increases the density of active sites thus increasing the ECSA of CoP/Co$_3$O$_4$. The largest ECSA of s-CoP/ Co$_3$O$_4$ further explains its best electro-catalytic activity towards water splitting. The electrochemically active surface areas (ECSA, @50 mV s^{-1}, Fig. S11†) normalized LSV curves of Co$_3$O$_4$, CoP, CoP/Co$_3$O$_4$, and s-CoP/Co$_3$O$_4$ are summarized in Fig. S12,† the results show that the intrinsic activity of active sites in s-CoP/Co$_3$O$_4$ is similar to that of Co$_3$O$_4$, CoP and CoP/Co$_3$O$_4$, indicating that the CoP coating and surface engineering process improve the catalytic performances of the electrode by creating new active sites towards OER rather than enhancing the intrinsic catalytic activity of active sites in Co$_3$O$_4$. Notably, the comparisons of overpotentials towards OER and HER of the as-prepared s-CoP/Co$_3$O$_4$ and transition metal-based catalysts in the latest literature reports are shown in Fig. 5d and e and Tables S1–S3,† which indicate that the s-CoP/Co$_3$O$_4$ performs competitive catalytic activities for both HER and OER.

To further characterize the effect of the NaBH$_4$ reduction process, X-ray absorption spectroscopy (XAS) was employed to characterize the Co K-edge in CoP and s-CoP. The X-ray absorption near-edge spectroscopy (XANES) spectra in Fig. 6a show that the Co K-edge adsorption energy of CoP is lower than that of CoO, yet higher than that of the Co foil, indicating that the average valence in CoP is lower than +2. Moreover, the absorption energy of Co K-edge in s-CoP gets lower relative to CoP, thus verifying the successful reduction of Co species, which does well to the OER process. This conclusion can be further verified by the fitting curve (Fig. S8†), the absorption energy of Co K-edge in s-CoP is lower than that of the fit curve. The Fourier-transformed (FT) k^2-weighted extended X-ray absorption fine structure (EXAFS) spectra of CoP and s-CoP at R space are shown in Fig. S9,† the main peak at 1.6 can be corresponded to Co–P coordination shells.[26] The peak corresponding to Co–P shifts from 1.62 to 1.65 in reduced CoP, which indicates the prolonged bond length and impaired interaction between Co and P atoms. Therefore, the reduction process decreases the chemical environment of P atoms, thus decreasing the adsorption energy of H to CoP, facilitating the H* desorption process in HER. Moreover, the peak intensity of Co–P decreases obviously in s-CoP, further indicating the increased degree of disorder and the formation of P vacancies.
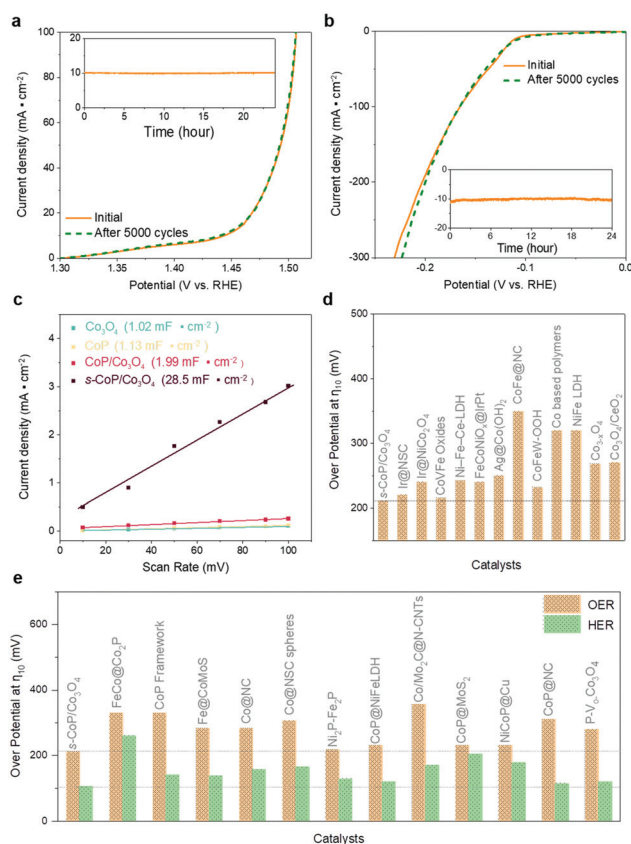

Fig. 5 (a and b) Polarization curves of s-CoP/Co$_3$O$_4$ recorded before and after 5000 CV cycles, (c) C_{dl} values of Co$_3$O$_4$, CoP, CoP/Co$_3$O$_4$ and s-CoP/Co$_3$O$_4$ in 1 M KOH, comparison of overpotentials of s-CoP/ Co$_3$O$_4$ and other catalysts reported in the latest literature reports towards (d) OER and (e) OER and HER at η$_{10}$ in 1 M KOH.
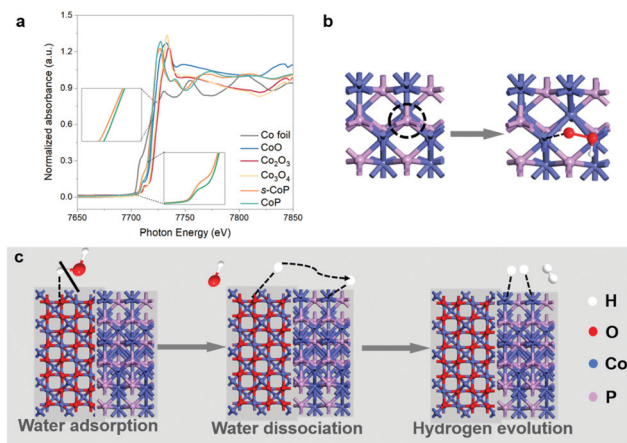
Fig. 6 (a) X-ray absorption near–edge spectroscopy (XANES) spectra of Co K-edge of CoP, r-CoP and reference materials (Co foil, CoO, Co_2O_3 and Co_3O_4), (b) promotion mechanism of unsaturated Co sites towards OER, (c) illustration of the HER process in the alkaline environment on the CoP/Co_3O_4 electrode.

The effects of s-CoP in HER and OER can be presumed as shown in Fig. 6b and c according to the electro-catalytic performances of the as-prepared materials and previous research projects. In the oxygen evolution process, electron-deficient Co atoms in CoP act as the adsorption sites towards electro-negative reactants and intermediates, thus providing dual active sites towards OER. It has been reported that anionic vacancies will decrease the activation energy of OER,[27] thus the P vacancies also act as the active sites towards OER. In the HER process, the catalytic reaction takes place in a tandem pathway,[28] in which Co_3O_4 catalyzes the water dissociation process while the CoP catalyzes the hydrogen evolution process.[29] The normalized turnover frequency (TOF) calculations have been involved to verify the speculation. The detailed calculation process has been added to the revised ESI,† where the number of active sites are estimate by ECSA of the as-prepared materials (Fig. S11,† @50 mV s^{-1}). The results in Fig. S13 and S14† show that the normalized TOF of s-CoP/Co_3O_4 is similar to that of CoP and CoP/Co_3O_4 while slightly better Co_3O_4 in OER, indicating that the s-CoP enhances the catalytic performance of the electrode mainly by increasing the density of active sites in OER. Conversely, the intrinsic catalytic activity of active sites in s-CoP/Co_3O_4 is obviously better than other materials in HER process, suggesting that the involvement of Co_3O_4 and surface engineering process enhances the catalytic performance of CoP not only by enlarging the density of active sites. Therefore, the s-CoP/Co_3O_4 shows excellent catalytic activity towards water splitting in alkaline environment.

Conclusions

In this work, layered Co_3O_4 was synthesized by thermal treatment of $Co(OH)_2$, then the CoP nanolayer was coated on the surface of Co_3O_4 by electrodeposition, forming a heterojunction structure. The CoP/Co_3O_4 is further reduced by $NaBH_4$ solution to obtain anionic vacancies at the surface of s-CoP/Co_3O_4, which was used as the electrode towards water splitting in an alkaline environment. The vacancies cause fewer electropositive Co atoms, promoting oxygen evolution. It can be presumed that in the HER process, the s-CoP/Co_3O_4 electrode catalyzes reaction *via* a tandem reaction pathway and the s-CoP/Co_3O_4 offers dual active sites in the OER process. The current density of 10 mA cm^{-2} can be obtained at only 211 and −106 mV *vs.* RHE for OER and HER, respectively. This study provides a novel strategy to fabricate high-performance noble metal-free electrodes by involving efficient active sites for both OER and HER, which provide remarkable performance for water splitting in an alkaline environment.

Experiment section

Chemicals and materials

Cobalt nitrate hexahydrate ($Co(NO_3)_2 \cdot 6H_2O$, 98%), potassium hydroxide (KOH, 85%), sodium borohydride ($NaBH_4$, 98%), sodium hypophosphite monohydrate ($NaH_2PO_2 \cdot H_2O$, 98%), sodium citrate ($Na_3C_6H_5O_7$, 98%), potassium chloride (KCl, 98%), ethanol (C_2H_5OH, 95%) hydrochloric acid (HCl, 35%–37%), nitric acid (HNO_3, 98%) potassium hydroxide (KOH, 95%) were obtained from Aladdin Reagents Ltd (China) and used as received without further purification.

Materials preparation

Layered Co_3O_4 was synthesized by thermal treatment of $Co(OH)_2$. Specifically, $Co(NO_3)_2$ solution (0.01 g mL^{-1}, 150 mL) was firstly heated to 80 °C under vigorous stirring. Then, 150 mL KOH solution (20 mM) was added dropwise to the $Co(NO_3)_2$ solution and kept for 1 h. The solution was filtered and washed using DI water three times after cooling to room temperature. The sediment was dried in a vacuum at 50 °C overnight to obtain $Co(OH)_2$. Finally, the $Co(OH)_2$ powder was transferred to the muffle furnace and annealed for 2 h at 250 °C to obtain Co_3O_4. The s-Co_3O_4 was obtained by the surface engineering of Co_3O_4. Typically, the as-prepared Co_3O_4 powder (50 mg) was dispersed in 20 mL freshly prepared $NaBH_4$ solution (0.3, 0.5, 0.7 mM) for 1 h and then filtered, washed with DI water three times. The as-prepared powder was dried in vacuum at 50 °C for 24 h to obtain s-Co_3O_4. The working electrodes were fabricated by supporting the catalysts on the prepared carbon paper (the commercial carbon paper was first cut into pieces of 0.5 × 1 cm^2 and washed by sonication for 15 minutes in water, ethanol, and hydrochloric acid consecutively. After that, the carbon paper was pre-functionalized with HNO_3). Typically, 4 mg Co_3O_4 powder and 40 μL of 5 wt% Nafion solution were dispersed in 500 μL water and ethanol mixture solution ($V_{water} : V_{ethanol} = 3 : 2$). Then, 20 μL catalyst ink (containing 100 μg catalysts) was loaded onto a carbon paper and dried in the vacuum at 50 °C to obtain the Co_3O_4/CP electrode. The CoP layer was electro-deposited on

Co_3O_4/CP in 50 mL electrolyte containing 0.8 g Co $(NO_3)_2·6H_2O$, 0.3 g sodium citrate and 1 g $NaH_2PO_2·H_2O$ at a potential of −1.2 V (*vs.* Ag/AgCl) for 900 s at room temperature to obtain the CoP/Co_3O_4/CP electrode. During the electrodeposition process, the Ag/AgCl (3.5 M KCl) was employed as the reference electrode and the graphite rod was the counter electrode. The CoP/Co_3O_4 electrode was finally sunk in 20 mL freshly prepared $NaBH_4$ solution (0.3, 0.5, 0.7 mM) for 1 h and washed with DI water several times to obtain the s-CoP/Co_3O_4 working electrode.

Materials and electrochemical characterization

Raman spectra (Renishaw inVia confocal microscopy), X-ray powder diffraction (XRD, Bruker D2 Phaser), X-ray photoelectron spectroscopy (XPS, K-ALPHA), scan electron microscopy (SEM, QUATTRO S) and transmission electron microscopy (TEM, Philips Tecnai G2F20) were used for the characterization of the obtained materials. X-ray absorption spectroscopy (XAS, NSRRC BL17C1, following a previously published literature procedure[30]). Electrochemical measurements were performed on a CHI760E, workstation using a conventional three-electrode system with the sample loading on a carbon paper as the working electrode, Hg/HgO (1 M KOH solution) as the reference electrode and graphite rod as the counter electrode. The alkaline electrolyte was a 1 M KOH aqueous solution. All the measured potentials were calibrated to RHE by using the following equation: E(RHE) = E(Hg/HgO) + 0.098 V (25 °C) + 0.059 × pH.

Author contributions

Xintong Li and Zonglong Zhu developed the research idea. Xintong Li synthesized the materials, recorded the electrocatalytic performances, analyzed the characterization results and wrote the original version of the manuscript under the supervision of Zonglong Zhu. Yizhe Liu and Qidi Sun assisted with the experimental design and revision of the drafts while Zilong Wang helped to characterize the materials. Wei-Hsiang Huang characterized the as-prepared materials by XAS. Chu-Chen Chueh and Chi-Liang Chen helped to revise and edit the manuscript. Zonglong Zhu offered funding, revised and edited the manuscript.

Conflicts of interest

There are no conflicts to declare.

Acknowledgements

References

1 V. H. Hoa, D. T. Tran, D. C. Nguyen, *et al.*, *Adv. Funct. Mater.*, 2020, **30**, 2002533; L. Zhuang, Y. Jia, H. Liu, *et al.*, *Angew. Chem., Int. Ed.*, 2020, **59**, 14664–14670; T. Ling, D.-Y. Yan, Y. Jiao, *et al.*, *Nat. Commun.*, 2016, **7**, 12876.

2 Z. Li, J.-Y. Fu, Y. Feng, *et al.*, *Nat. Catal.*, 2019, **2**, 1107–1114; H. Sun, C. Tian, G. Fan, *et al.*, *Adv. Funct. Mater.*, 2020, **30**, 2004375.

3 Y. Pi, Y. Xu, L. Li, *et al.*, *Adv. Funct. Mater.*, 2020, **30**, 2004375.

4 C. Liang, P. Zou, A. Nairan, *et al.*, *Energy Environ. Sci.*, 2020, **13**, 86–95; B. Shan, M. K. Brenneman, L. Troian-Gautier, *et al.*, *J. Am. Chem. Soc.*, 2019, **141**, 10390–10398.

5 M. A. Ahsan, A. R. P. Santiago, Y. Hong, *et al.*, *J. Am. Chem. Soc.*, 2020, **142**, 14688–14701.

6 H. Huang, A. Cho, S. Kim, *et al.*, *Adv. Funct. Mater.*, 2020, **30**, 2003889.

7 J. Yin, J. Jin, M. Lu, *et al.*, *J. Am. Chem. Soc.*, 2020, **142**, 18378–18386.

8 K. Yuan, D. Luetzenkirchen-Hecht, L. Li, *et al.*, *J. Am. Chem. Soc.*, 2020, **142**, 2404–2412.

9 H. Huang, S. Zhou, C. Yu, *et al.*, *Energy Environ. Sci.*, 2020, **13**, 545–553; Y. Guo, J. Tang, J. Henzie, *et al.*, *ACS Nano*, 2020, **14**, 4141–4152; Q. Lian, L. Zhong, C. Du, *et al.*, *ACS Nano*, 2019, **13**, 7975–7984.

10 Q. Shi, Q. Liu, Y. Ma, *et al.*, *Adv. Energy Mater.*, 2020, **10**, 2002896; L. L. Ji, J. Y. Wang, X. Teng, *et al.*, *ACS Catal.*, 2020, **10**, 412–419; Z. Y. Zhang, X. X. Zhao, S. B. Xi, *et al.*, *Adv. Energy Mater.*, 2020, **10**, 1902854; Y. Liu, X. Wu, X. Guo, *et al.*, *Mater. Today Energy*, 2021, **19**, 100610.

11 H. W. Huang, S. Zhou, C. Yu, *et al.*, *Energy Environ. Sci.*, 2020, **13**, 545–553.

12 A. Moysiadou, S. Lee, C. S. Hsu, *et al.*, *J. Am. Chem. Soc.*, 2020, **142**, 11901–11914; J. Liu, Y. Ji, J. Nai, *et al.*, *Energy Environ. Sci.*, 2018, **11**, 1736–1741; M. Kuang, J. Zhang, D. Liu, *et al.*, *Adv. Energy Mater.*, 2020, **10**, 2002215.

13 B. Zhang, L. Wang, Z. Cao, *et al.*, *Nat. Catal.*, 2020, **3**, 985–992; P. W. Menezes, C. Panda, C. Walter, *et al.*, *Adv. Funct. Mater.*, 2019, **29**, 1808632.

14 R. Zhang, Y.-C. Zhang, L. Pan, *et al.*, *ACS Catal.*, 2018, **8**, 3803–3811; Y. Wang, T. Zhou, K. Jiang, *et al.*, *Adv. Energy Mater.*, 2014, **4**, 1400696; K.-Y. Niu, F. Lin, S. Jung, *et al.*, *Nano Lett.*, 2015, **15**, 2498–2503; L. Xu, Q. Jiang, Z. Xiao, *et al.*, *Angew. Chem., Int. Ed.*, 2016, **55**, 5277–5281.

15 G. Zhou, M. Li, Y. Li, *et al.*, *Adv. Funct. Mater.*, 2020, **30**, 1905252.

16 L. Ji, J. Wang, X. Teng, *et al.*, *ACS Catal.*, 2020, **10**, 412–419.

17 X.-W. Lv, Y. Liu, R. Hao, *et al.*, *ACS Appl. Mater. Interfaces*, 2020, **12**, 17502–17508.

18 X. Wang, X. Li, J. Mu, *et al.*, *ACS Appl. Mater. Interfaces*, 2019, **11**, 41988–41999.

19 C. Tang, R. Zhang, W. B. Lu, *et al.*, *Adv. Mater.*, 2017, **29**, 1602441; Z. Xiao, Y. Wang, Y.-C. Huang, *et al.*, *Energy Environ. Sci.*, 2017, **10**, 2563–2569.

20 G. Dong, H. Hu, X. Huang, *et al.*, *J. Mater. Chem. A*, 2018, **6**, 21003–21009; Q. Wang, X. Xue, Y. Lei, *et al.*, *Small*, 2020, **16**, 2001571.

21 Z.-H. Xue, H. Su, Q.-Y. Yu, *et al.*, *Adv. Energy Mater.*, 2017, **7**, 1602355.

22 Z. Li, Y. Zhang, Y. Feng, *et al.*, *Adv. Funct. Mater.*, 2019, **29**, 2000364; Y. Liu, C. Ma, Q. Zhang, *et al.*, *Adv. Mater.*, 2019, **31**, 1900062.

23 R. Boppella, J. Tan, W. Yang, *et al.*, *Adv. Funct. Mater.*, 2019, **29**, 1807976.

24 X. Zhou, H. Gao, Y. Wang, *et al.*, *J. Mater. Chem. A*, 2018, **6**, 14939–14948.

25 Z. Chen, Y. Ha, H. Jia, *et al.*, *Adv. Energy Mater.*, 2019, **9**, 1807976; M. Li, Y. Zhu, H. Wang, *et al.*, *Adv. Energy Mater.*, 2019, **9**, 1803918.

26 E. Cao, Z. Chen, H. Wu, *et al.*, *Angew. Chem., Int. Ed.*, 2020, **59**, 4154–4160.

27 Z. Xiao, Y.-C. Huang, C.-L. Dong, *et al.*, *J. Am. Chem. Soc.*, 2020, **142**, 12087–12095.

28 C. Tang, Y. Zheng, M. Jaroniec, *et al.*, *Angew. Chem., Int. Ed.*, 2021, **60**, 2–21.

29 S. Anantharaj, S. Noda, V. R. Jothi, *et al.*, *Angew. Chem., Int. Ed*, 2021, **60**, 2–28.

30 W.-H. Huang, W.-N. Su, C.-L. Chen, *et al.*, *Appl. Surf. Sci.*, 2021, **562**, 1873–5584.